Improving Seismic Resolution Through Array Processing Techniques

Sebastian Rost · Christine Thomas

Abstract Seismic arrays, first introduced in the late 1950s to detect underground nuclear explosions, have helped to improve our knowledge about the structure of the Earth for the last 40 years. During these years, numerous array processing methods have been developed that use the high signal coherence and accurate timing of array data to generate high-resolution images of Earth structure. Here, we present an overview of resolution issues related to seismic array studies of Earth structure by first introducing basic array processing techniques and then discussing more advanced techniques applied to array data recently. The increase of seismic stations deployed in experiments or permanently in many regions of the globe allows a much denser sampling of the seismic wavefield. This dense sampling enables the adaptation of controlled source analysis techniques for the study of Earth structure using earthquakes with higher resolution than previously possible. Here we will discuss different migration methods of teleseismic data that use the incidence angle information of scattered arrivals to obtain images of Earth structure. Finally, we show data examples how these methods can be used to increase our knowledge of the structure of the Earth's deep interior.

Keywords Seismic array · Seismic resolution · Deep earth structure · Seismic processing

S. Rost (✉)
School of Earth and Environment, Institute of Geophysics and Tectonics, The University of Leeds, Leeds LS2 9JT, UK
e-mail: s.rost@leeds.ac.uk

C. Thomas
Department of Earth and Ocean Sciences, University of Liverpool, 4, Brownlow Street, Liverpool L69 3GP, UK

Present Address:
C. Thomas
Institut für Geophysik, Westfälische Wilhelms Universität Münster, Münster, Germany

1 Introduction

Arrays of sensors are widely used in the physical sciences [e.g., acoustics (Williams et al. 1980) or radio-astronomy (Tarenghi 2008)] to increase signal strength and gaining directivity information of signals. Arrays to record and analyze elastic waves of the Earth have been developed since the late 1950s to test the ability to monitor underground nuclear explosions (Carpenter 1965). It has been demonstrated that seismic arrays are superior to three-component single stations in detecting and locating seismic sources (natural and man-made). In the last 40 years numerous seismic arrays have been installed around the globe and array data have been used both to monitor compliance with the Comprehensive Test Ban Treaty (CTBT) as well as for fundamental research.

No strict definition of a seismic array exists, but all arrays allow a means of analysis of the data as an ensemble rather than individual channels (Rost and Garnero 2004) and normally have a common time signal (Davies et al. 1971) allowing accurate differential timing between the individual array elements. In general, array data show high signal coherency across the whole array aperture as well as low coherency of noise between the individual stations. Recently, large networks of seismometers have been installed to study Earth structure (e.g., GHENGIS, (Roecker 2001); EAGLE (Bastow et al. 2005); CANOE (Mercier et al. 2008); USARRAY (Henyey 2000), to name a few) and have proven their ability to resolve the structure of the Earth in great detail. A seismic array differs from a seismic network mainly in the way the data are processed (Schweitzer et al. 2002), but the high signal coherency that is required for most seismic array methods puts constraints onto the usability of network data for array processing. Signal coherency is dependent on local structure and noise conditions, on array design and on the frequency content of the signal of interest. Therefore, many different array configurations that have been optimized for specific purposes exist (Haubrich 1968). Even more important for most array processing algorithms that use the small differences in delay times between stations (Rost and Thomas 2002) is the accuracy of time measurements between individual stations. The processing tools require small timing uncertainties between the individual channels of a network or array. Due to the common time base of seismic arrays this does not pose a problem with array data. This prerequisite becomes less demanding since the GPS time signal commonly used for seismic networks are highly accurate, but care must be taken to avoid timing errors (e.g., time drifts between GPS synchronization) in these data.

The advantage of seismic arrays compared to individual stations is two-fold: (1) arrays allow an increased signal-to-noise ratio (SNR) of the seismic signal due to time series stacking and suppression of incoherent noise; (2) arrays allow estimates of the directivity of the recorded signal, i.e., due to the three-dimensional sampling of the seismic wave field arrays can determine the slowness vector of the arriving wave field. The details of this array property will be given in Sect. 3. With these advantages arrays are valuable for source location determination using the slowness vector. Directivity information as well as improved SNR of subtle arrivals in the seismic wave field of stacked array data also proved useful for structural analysis. Numerous methods exist to this end (see reviews by Rost and Thomas (2002) and Schweitzer et al. (2002) and references therein).

This review introduces a brief overview of conventional array methods, such as beamforming, slant stacks or vespagrams and methods that can determine the slowness and backazimuth simultaneously. Following the overview, we will discuss the resolution of seismic observations with arrays and their influence on the seismic Fresnel zone. To document the ability to enhance the resolution in seismic array studies, we will then introduce some seismic migration methods that are used in deep Earth seismology. In a

final section, we will show some examples of array techniques and resolution of seismic data on selected examples as well as potential problems when using array methods for non-standard phases that are not predicted by radial Earth models.

2 Overview of Traditional Array Techniques

2.1 Introduction

Most array methods assume that the energy arriving at the array can be approximated as a plane wavefront. This is a good assumption for most arrivals from teleseismic source-receiver distances, but breaks down for local distances where source and array are separated by less than a few array apertures, where the wavefront is curved, and for phases originating close to the array such as scattered energy (Thomas et al. 1999) or P-wave to Rayleigh wave conversions (Clouser and Langston 1995).

An array consists of an assembly of individual seismic stations. Each station (or element) location can be described by a position vector r_j. The propagation direction of the wavefront arriving at an array is commonly described by two parameters (Fig. 1) (1) the vertical incident angle i and (2) the backazimuth θ. The backazimuth θ describes the horizontal angle of incidence of the incident wavefront measured clockwise from north, i.e., the direction of the great circle path connecting source and array. The vertical incident angle i is not routinely used in array studies, but is transferred into the observable apparent velocity of the wave front across the array v_{app}, with:

$$\frac{1}{v_{app}} = \frac{\sin i}{v_0} = u \tag{1}$$

with v_0 as the velocity beneath the array and u being the slowness.

Both parameters are commonly combined into the slowness vector $\boldsymbol{u}$. In a spherical geometry, $\boldsymbol{u}$ is defined as:

$$\begin{aligned}
\boldsymbol{u} &= (u_x, u_y, u_z) \\
&= \left(\frac{\sin \theta}{v_{app}}, \frac{\cos \theta}{v_{app}}, \frac{1}{v_{app} \tan i} \right) \\
&= u_{hor} \left(\sin \theta, \cos \theta, \frac{1}{\tan i} \right) \\
&= \frac{1}{v_0} (\sin i \sin \theta, \sin i \cos \theta, \cos i)
\end{aligned} \tag{2}$$

where u_x is usually measured along the EW direction, u_y in the NS direction.

The slowness vector $\boldsymbol{u}$ points into the direction of wave propagation and its modulus is the reciprocal of the wave speed. Horizontal slowness u_{hor} is dependent on the ray parameter p and R_0 is the turning distance of the ray from the Earth's centre. For a 'spherical' Earth:

$$p = \frac{r \sin i}{v} = \frac{R_0 \sin i}{v_0} = R_0 u_{hor} \tag{3}$$

with v_0 the velocity at R_0.
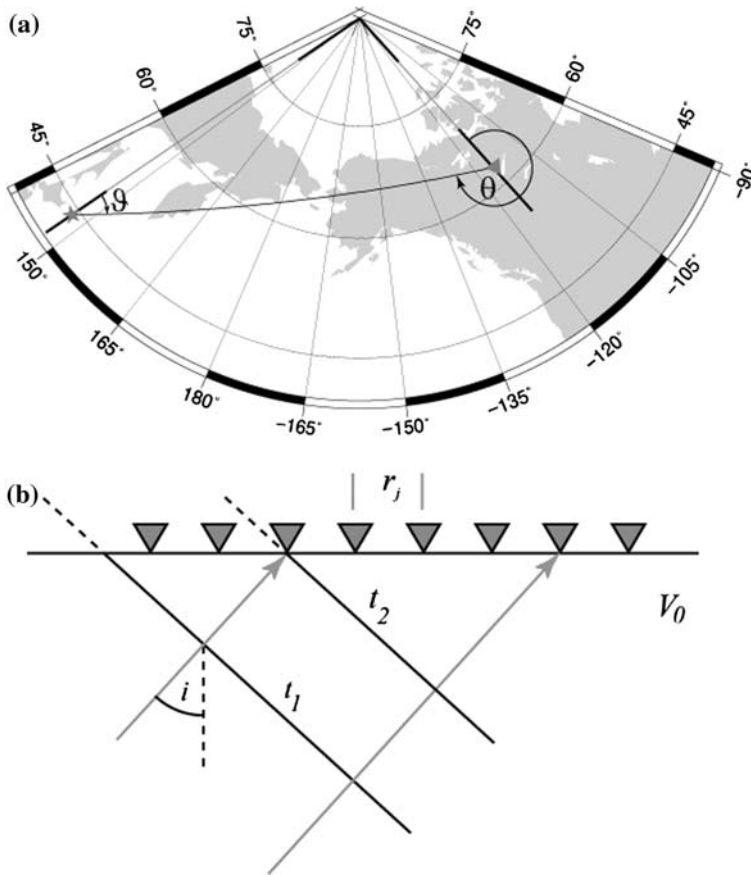
Fig. 1 **a** Sketch of definition of backazimuth θ as the angle against North of the great circle path connecting receiver (*triangle*) and source (*star*) measured at the receiver. In contrast, the azimuth ϑ is defined as the angle of the great circle path against North as seen from the source. **b** Sketch of the definition of the incident angle i used to define the slowness parameter u. Due to the incident angle the plane wavefront travels across an array at the surface with an apparent velocity v_{app} dependent on the incident angle i. Since the array station locations are known this can be used to calculate the slowness. r_j are the locations of the stations from the centre station

Although the slowness vector is three-dimensional, in most cases the elevation differences between the individual array elements are small and the vertical component of the slowness vector u_z cannot be measured.

Due to the discrete locations of the elements of the array, an incoming wavefront will arrive with small time offsets (or delay times) t between the stations, which depend on the slowness vector u and the station location (characterized by the location vector r_j):

$$t_j = r_j \cdot u. \tag{4}$$

Measuring the time delays t_j between individual stations and knowing the station locations r_j therefore allows a direct measure of the slowness vector u. The accuracy of the measurement of the slowness vector depends on the quality of the timing between the station (i.e., the absence of time drift between the array stations) and on the station location

(Fig. 2), i.e., the array characteristics (Fig. 2) (Haubrich 1968; Mykkeltveit et al. 1983; Harjes 1990).

2.2 Beamforming, Slant Stacks, Vespagrams

An important advantage of seismic arrays over single stations is their ability to increase the ratio of the coherent signal over incoherent noise, therefore increasing the SNR. The arrival times for a seismic wave at each station can be estimated for each angle of incidence and hence it is possible to stack the recordings of the individual stations to enhance arrivals with known slowness u and/or backazimuth θ by taking the interstation delay times into account before stacking. This process is called beamforming or 'delay-and-sum' technique (Harjes and Henger 1973; Rost and Thomas 2002; Schweitzer et al. 2002).

To perform beamforming, the recordings of the individual array stations x_j are shifted in time with the appropriate delay times t_j for the angle of incidence i, i.e., the slowness and backazimuth and the station location ($t_j = t_j(\mathbf{r_j}, u, \theta)$). The time shifted traces are then summed or stacked yielding the beam trace $b(t)$:

$$b(t) = \frac{1}{M} \sum_{j=1}^{M} x_j(t + t_j). \tag{5}$$

where t_j is the delay time for the j-th station relative to an array reference point, x_j the recording at the j-th station and M the number of stations within the array. If the trace x is composed of a coherent signal s and noise n ($x(t) = s(t) + n(t)$), this will yield:

$$b(t) = s(t) + \frac{1}{M} \sum_{j=1}^{M} n_j(t + t_j), \tag{6}$$

assuming a perfectly coherent signal $s(t)$. With uncorrelated noise n_j at the individual stations the time shifted noise terms do not sum up constructively, therefore reducing the noise amplitude by a factor of $\sqrt{M}$ compared to the signal (Rost and Thomas 2002).

Beamforming relies on a number of assumptions: (1) the signal must be coherent across the whole array, (2) the signal arrives as a planar wavefront, and (3) the noise field is uncorrelated to achieve a $\sqrt{M}$ noise reduction. Smaller noise reduction is possible in case of slightly correlated noise.

Signal coherency is dependent on wavelength and array aperture, i.e., the signal coherency can rapidly decay if the aperture of the array is too large compared to the wavelength of the signal. If the noise field is correlated (Friedrich et al. 1998) a weighting factor can be applied to the traces prior to summing (Johnson and Dudgeon 1992) to mitigate the effects of the coherent noise.

An example of array recordings showing the signal coherency between the stations and a beam trace is shown in Fig. 3. An array beam is formed for a specified slowness and backazimuth (e.g., a P-wave from a known source location for slowness determination) and these incident angles must be known. The calculated time delays assume a homogeneous underground beneath the array, which is not a good approximation for some arrays. Structural inhomogeneities in the array underground influence the travel times to individual stations, therefore leading to additional time differences which have to be taken into account for a successful beam. To this end, array mislocation vectors have been determined for some arrays (Bondar et al. 1999; Krüger and Weber 1992) that allow corrections taking the local structure underneath the array stations into account.
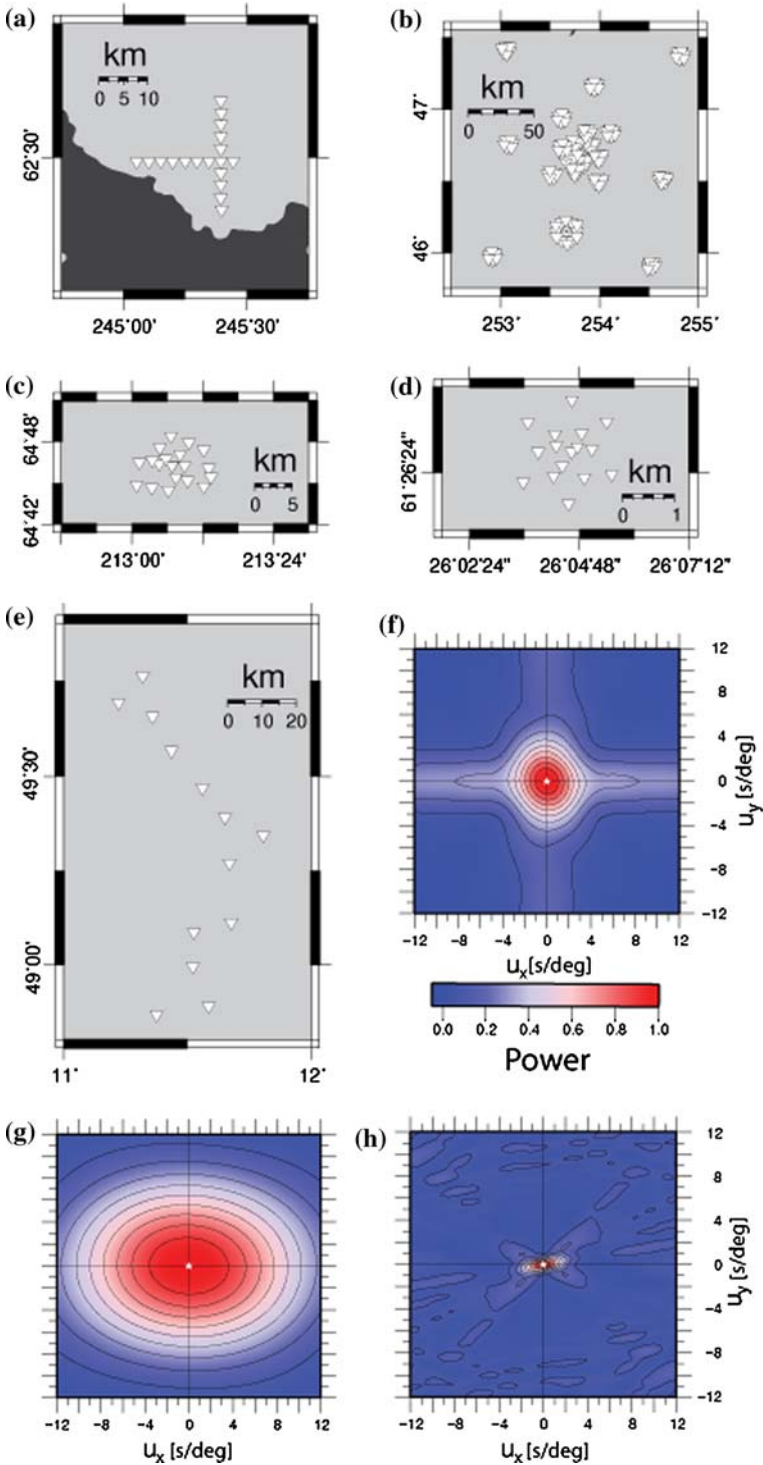
◄ **Fig. 2** Examples of array configurations. Arrays are commonly designed for specific purposes (e.g., nuclear explosion monitoring) and to work in a certain frequency range. Therefore, different designs evolved over time. Examples are: **a** Yellowknife array (YKA) configuration. YKA is a UK type array with about 20 stations deployed along two approximately perpendicular branches. Other examples of the UK type are Eskdalemuir (UK), Gauribidanur (India), and Warramunga (Aus). **b** Large Aperture Seismic Array (LASA) configuration. An experimental array located in Wyoming (US) which operated from 1965 to approximately 1978 (Green et al. 1965). With an aperture of approximately 200 km with up to 630 short-period stations it was a massive array built to monitor underground nuclear tests. Stations were deployed in subarrays located on concentric circles. A similar (though smaller) array of this type is NORSAR in Norway. **c** Eielson array (ILAR) configuration in Alaska (US). Similar to LASA, stations are deployed on concentric circles, but with fewer stations (about 20) and an aperture of only about 10 km. **d** GERESS configuration from Germany. Similar to ILAR but with a smaller aperture of 3 km. ILAR and GERESS are arrays of the recent CTBTO design. **e** Gräfenberg array (GRF) configuration. An array purely equipped with broadband seismometers. The asymmetric shape follows the local geology to ensure signal coherency. Depending on the array design and the station locations the receiver characteristics of the arrays differ. The characteristics are given by the array response function (ARF). Examples are given for **f** YKA array response function calculated for data with a dominant frequency of 1 Hz. **g** ILAR ARF calculated for synthetic data with a dominant frequency of 10 Hz. **h** GRF ARF calculated for synthetic data with a dominant frequency of 1 Hz. For the ARFs the slowness components u_x and u_y are given instead of the wavenumbers k_x and k_y

Other methods to measure the slowness vector of incoming seismic energy have been developed both for source location and phase identification (Schweitzer et al. 2002). These methods often use multiple beamforming processes for varying slowness or backazimuth values. The VESPA process (velocity spectral analysis) (Davies et al. 1971) calculates array beams for varying slownesses (and constant backazimuth) but can also be expanded to work with varying backazimuth (and constant slowness). The vespagram traces $v(t)$ for a range of slowness values ($\zeta_{min} \leq \zeta \leq \zeta_{max}$) for a fixed backazimuth θ can be written as:

$$v_\zeta(t) = \frac{1}{M} \sum_{j=1}^{M} x_j(t + t_{j,\zeta}) \tag{7}$$

where again $t_{j,\zeta}$ is the delay time at the j-th station for a specific slowness ζ. Care must be taken in this approach that the fixed azimuth or slowness is close to the true value since deviations from the true backazimuth or slowness can lead to misleading measurements of the variable parameter (Rost and Thomas 2002).

To achieve better slowness resolution, it is possible to stack the traces using the n-th root stacking technique (Kanasewich et al. 1973; Muirhead and Datt 1976; McFadden et al. 1986), a non-linear stacking method in which the signal to noise ratio is improved but the waveform is distorted. This method takes the n-th root of the traces, shifts them in time according to slowness and backazimuth and after stacking the shifted traces takes the beam trace to the power of n, with $n = 2,3,\ldots$ The sign of each sample is preserved in this process and therefore polarities of the stacked waves are correct. Taking the n-th root of the individual traces effectively reduces the amplitude variance of the trace. In effect, the processing puts more emphasis on the coherency of the signal than on the amplitudes. Taking the n-th power after the summation enhances the amplitude differences again. Since taking the n-th root is a nonlinear process, the waveforms are distorted and waveform information in the vespagram can no longer be used except for polarities of arrivals. Figure 3b shows a fourth root slowness-vespagram of an earthquake on Nov. 11, 1993 00:28 recorded at the medium aperture Yellowknife array in Northern Canada with the arriving P-wave slowness close to the predicted slowness for a 1D Earth model. Incoherent noise on the traces has been reduced and coherent P-coda phases have been
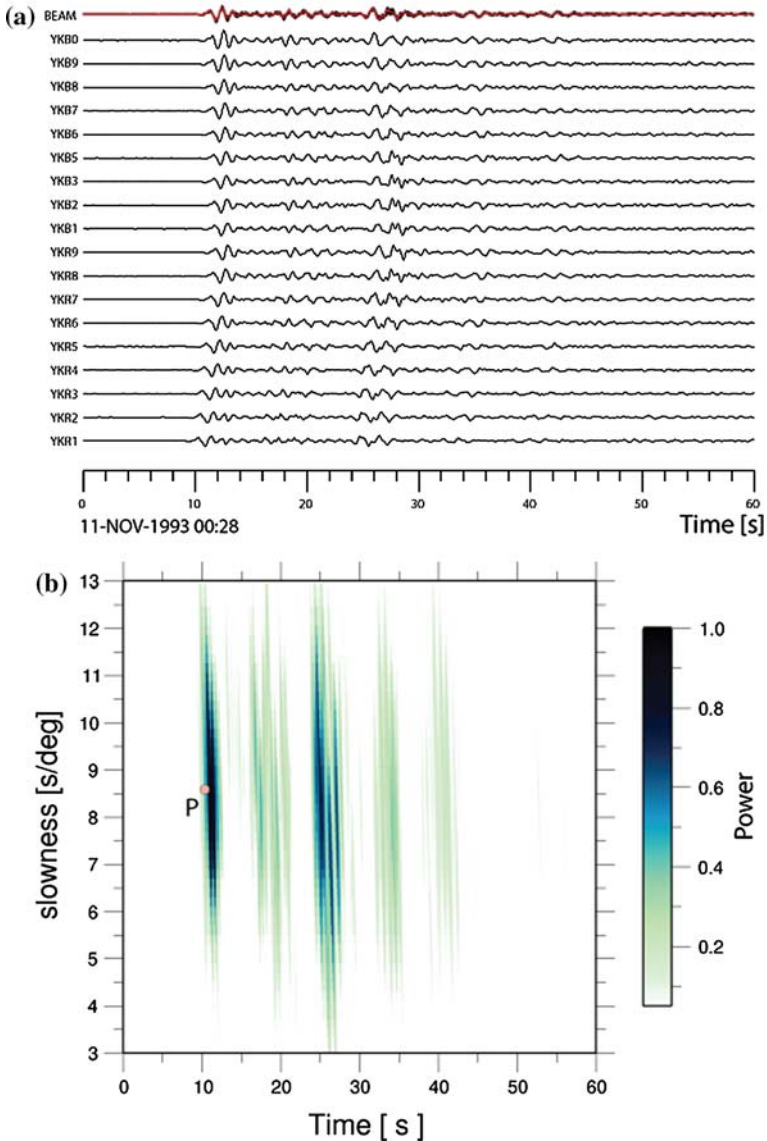
Fig. 3 Example of signal coherency for an event from the Kuriles recorded at YKA. **a** Raw seismic waveforms for the individual YKA station as recorded (i.e., without taking the time delays into account). The beam trace together with an overlay of all recordings taking the time delays due to the station location into account is shown in red on the top of the figure. **b** 4th root vespagram of the event data shown in (**a**). The vespagram allows the identification of the slowness of the first *P*-arrival which is approximately 8.7 s/deg and other later *P*-coda arrivals

mapped in slowness-time space. Other non-linear stacking techniques using coherency measurements exist and work in a similar way (Schimmel and Paulssen 1997; Mohan and Rai 1992).

2.3 Simultaneous Slowness and Backazimuth Measurement

Many array methods to study Earth structure assume that the seismic energy travels along the great circle path (gcp) connecting source and receiver. For waves that travel out of plane (deviations from the assumed great circle path for source and receiver) their backazimuth will differ from theoretical values for the gcp for 1D Earth models. Such waves could be generated through scattering or reflections off lateral inhomogeneities. It is also possible that high- and low-velocity regions can refract waves and introduce deviations in slowness and/or backazimuths [e.g., (Kaneshima and Helffrich 1998; Weber and Wicks 1996; Rost et al. 2008; Kito et al. 2008)]. For such waves it is necessary to determine slowness and backazimuth simultaneously. Several methods have been developed to analyze seismic energy without the restriction to the great circle path and many different stacking processes have been developed [for an overview see e.g., (Rost and Thomas 2002)]. Examples of these methods are the frequency-wavenumber analysis (Capon 1969; Harjes and Henger 1973) which works in the spectral domain, the slowness-backazimuth analysis [also called beaman, beam power analysis, (King et al. 1976)], or beampacking analysis (Earle and Shearer 1998; Schweitzer et al. 2002) and are described in detail elsewhere (Rost and Thomas 2002; Schweitzer et al. 2002).

2.4 Double Array Stacking Techniques

When seismic arrays are discussed, in general only seismic receiver arrays are taken into account. Due to the reciprocity principle that allows a swap of source and receiver one can also use source arrays (Niazi 1969), i.e., several sources recorded at one receiver and the same mathematical principles can be applied as for the receiver arrays (Spudich and Bostwick 1987; Scherbaum et al. 1991). The improvement of the SNR for source arrays is similar to receiver arrays, although some care must be taken to normalize the different source mechanisms, e.g.. through source deconvolution. An inherent problem of source array studies is the required accuracy of source locations that is necessary for applying array processing techniques.

A combination of source and receiver arrays leads to a further improvement of the SNR due to the combined higher number of sources in the source array and receivers in the receiver array. Several names such as double array stacking (Revenaugh and Mendoza 1996; Reasoner and Revenaugh 1999; Kito and Krüger 2001) or double beam method (Krüger et al. 1996; Krüger et al. 1993) have been used to describe these methods. The double beam method has been described in detail by Krüger et al. (1993).

Recently the double array method finds much application in the exploration of the deep Earth with many studies targeting the D″ discontinuity at approximately 2600 km depth e.g., (Hutko et al. 2006; Lay et al. 2006; Avants et al. 2006; Reasoner and Revenaugh 1999). The double array stacking requires a target phase to calculate a theoretical move-out for a certain Earth model. For studies of the deep Earth the target phase is normally the specular reflection of the D″ discontinuity (SdS or PdP) of a core reflected phase (PcP or ScS) but it is also possible to use other phases like underside reflections off the upper mantle discontinuities (PdP or SdS). The stack S(d) is the sum of all traces for all events, therefore, combining source and receiver arrays, along the predicted move-out time (Reasoner and Revenaugh 1999):

$$S(d) = \sum_i \sum_j x_{ij} \left(\tau_0 + \tau_{ij}^{\text{tg}}(d) - \tau_{ij}^{\text{ref}} \right) \tag{8}$$

where x_{ij} is the recording of the jth station of event i, τ_0 is the traveltime required for alignment on e.g., the first arrival P which is necessary to align recordings of different earthquakes, τ_{ij}^{tg} is the predicted moveout for the target phase and τ_{ij}^{ref} the reference time for a target phase (in case of PdP generally P is used due to the small PcP amplitudes in many distance ranges, for SdS the core reflection ScS can be used). $S(d)$ represents a linear stack of the recordings of many events at many stations for a certain target depth d (e.g., the assumed depth of a D'' reflector or an assumed discontinuity depth) with no weighting of the individual traces being applied.

There are several ways the traces can be weighted before stacking, e.g., due to signal to noise ratio or for coherence of the signal. Kito and Krüger (2001) introduced a method to apply weighting to the stacked trace based on an amplitude independent measure of coherency based on the instantaneous phase of the signal (Sheriff and Geldart 1995; Schimmel and Paulssen 1997) and semblance as an amplitude dependent measure of coherency (Kito and Krüger 2001): the Phase stack $c(t)$ as stack of two analytic traces Z_1 and Z_2 is defined as (Schimmel and Paulssen 1997):

$$Z(t) = s(t) + i\mathrm{H}(s(t)) = A(t)\exp[i\Theta(t)]$$
$$c(t) = \frac{1}{M} \left| \sum_{j=1}^{M} \exp[i\,\Theta_j(t)] \right| \tag{9}$$

with $Z(t)$ being a complex trace, $s(t)$ being the original signal, M the number of traces used in the stack and H indicating the Hilbert transform of the signal s. $A(t)$ is the signal amplitude envelope and $\Theta(t)$ the instantaneous phase (Bracewell 1965; Schimmel and Paulssen 1997). The phase stack $c(t)$ does not contain any amplitude information, but is an amplitude independent measure of coherency (Schimmel and Paulssen 1997).

Semblance is an amplitude dependent measure of coherency and is defined as (Neidell and Taner 1971):

$$S(t) = \frac{\sum_{j=t_1(i)}^{t_2(i)} \left(\sum_{i=1}^{M} f_{ij} \right)^2}{M \sum_{j=t_1(i)}^{t_2(i)} \sum_{i=1}^{M} f_{ij}^2} \tag{10}$$

with f_{ij} being the data sample j at station i and $t_1(i)$ and $t_2(i)$ are the first and last sample of the time window for the computation of the semblance. $t_1(i)$ and $t_2(i)$ are chosen symmetrically around t and therefore the time window is parallel to the lag trajectory of the signal at t. Kito and Krüger (2001) define the phase-weighted semblance Ψ as the product of these two coherency measures:

$$\Psi(t) = S(t) \cdot c(t) \tag{11}$$

The phase-weighted semblance Ψ is multiplied with the beam power of the traces and provides a weighting based on their coherency as determined by the semblance and the instantaneous phase. The coherency weighting has the effect of an increased resolution since more coherent arrivals (i.e., the signal of interest) contribute more to the stack. Other weighting schemes using some signal properties can be used with similar effects (Neidell and Taner 1971).

3 Resolution

3.1 Array Configuration

The essential goal of an array is to resolve the seismic signal in frequency-wavenumber space. Different array configurations have been developed and are generally optimized for wave types, frequency, noise conditions and target region (especially for monitoring applications), with some example array configurations shown in Fig. 2. The cross shaped Yellowknife array in Canada is shown in Fig. 2a with the much larger Large Aperture Seismic Array (LASA) shown in Fig. 2b. Two modern circular arrays are shown in Fig. 2c, d (Eielson Array (ILAR), and the German GERESS array). A large broadband array [Gräfenberg Array (GRF)] that follows a dominant geological structure rather than resolution design constraints is shown in Fig. 2e. The resolution of the array is controlled by several factors of the configuration. A good measure of the receiver characteristics of an array is the array response function (ARF), which can be calculated as (Rost and Thomas 2002):

$$|A(\boldsymbol{k} - \boldsymbol{k}_0)|^2 = \left| \frac{1}{M} \sum_{j=1}^{M} e^{(2\pi i (\boldsymbol{k} - \boldsymbol{k}_0)) \cdot \boldsymbol{r}_j} \right|^2 \tag{12}$$

with $\boldsymbol{k}$ being the wavenumber vector of the incoming energy ($\boldsymbol{k_0}$ being the reference wavenumber vector), $\boldsymbol{r_j}$ the station location vectors and M the number of stations within the array

Equation 12 allows estimating the array response to an incoming wavefront with a slowness $\boldsymbol{u_0}$ (i.e., $\boldsymbol{k}_0$) but calculating the necessary time shifts for a slowness $\boldsymbol{u}$ (i.e., $\boldsymbol{k}$). As can be seen from Eq. 12 the ARF is a function of the array configuration defined by the location vectors $\boldsymbol{r_j}$, but it is also dependent on the wavenumber $\boldsymbol{k}$ (i.e., the wavelength or frequency of the incoming energy). Examples of array response functions for different array types are shown in Fig. 2f–h.

Since, the relative location of the stations within an array is essential for the receiver characteristics, and ultimately the ability of the array to locate a source or separate signals with different slownesses, care has to be taken when designing an array. The general rules for the resolution of arrays are (Rost and Thomas 2002; Schweitzer et al. 2002):

1. The aperture of an array controls the sharpness of the main lobe, i.e., it restricts the resolution of the wavenumber, i.e., for larger apertures, smaller wavenumbers can be measured. Wavelengths larger than the array aperture cannot be analyzed since in these cases the array acts like a single station.
2. The inter-station spacing defines the location of sidelobes of the ARF due to spatial aliasing.
3. The number of elements controls the suppression of energy with differing slowness crossing the array simultaneously, i.e., it defines the resolution of velocity, i.e., the ability of the array to act as a wavenumber filter.
4. The configuration defines the azimuthal dependence of the measurements.

Ideally the ARF should show a maximum as close to a δ-impulse as possible, strong suppression of energy outside of the main lobe of the ARF (i.e., good suppression of side lobes) and existing sidelobes should be outside of the wavenumber range of interest. An ARF should show very little azimuth dependence, i.e., the array can determine slowness and backazimuth with high precision independent of backazimuth. As an example the UK

type arrays (e.g., YKA, Fig. 2f) show strong sidelobes and a spread-out maximum and the receiver characteristics are strongly azimuth dependent, therefore not giving an ideal resolution. The modern arrays of the International Monitoring System (IMS) such as Eielson or GERESS show a much more δ-like ARF with little or no backazimuth dependence (Fig. 2g), although their resolution is restricted by their small aperture. GRF with its asymmetrical shape and large aperture shows an ARF between these two end members (Fig. 2h) with high resolution δ-peak like maximum, but some sidelobes and azimuth dependent resolution changes.

This discussion shows that the array configuration will have a tremendous influence on the possible resolution of an array. The possible resolution due to the array configuration is also frequency dependent. If the array aperture is of the same order as the wavelength the array can lose its detection capabilities as an array and works as a single station. On the other hand, if the wavelengths are too short the signal coherency between stations might be insufficient for the application of array analysis methods.

3.2 The Fresnel Zone

The concept of seismic Fresnel zones is closely related to similar effects in optics. The size of the Fresnel zone gives an estimate for the lateral resolution of seismic data. Simply put, for a reflected wave, a portion of the reflector rather than a single point is involved in producing the reflected energy (Hagedoorn 1954; Sheriff 1980). In essence, the difference between reflection point and Fresnel zone is that of ray theory versus seismic waves with a finite wavelength. The first Fresnel zone is the portion of a reflector from which reflected energy can reach a detector within the first half cycle of the signal and can therefore interfere constructively (Sheriff 1980). Energy arriving from within an area leading to a phase delay of the next half cycle on the other hand will interfere destructively at the receiver. Several ways exist to estimate the size of Fresnel zones for a variety of settings (Sheriff 1980; Gelchinsky 1985; Eaton et al. 1991; Knapp 1991) and are also described in introductory textbooks for exploration seismology.

In the context of seismic resolution of structures within the Earth it is important to point out that the Fresnel zone for a reflection is the cross section of the Fresnel volume around a ray with the reflector. Several methods take the finite volume of the ray into account for the calculation of synthetic seismograms (Cerveny and Soares 1992), the calculation of tomographic images (Husen and Kissling 2001), and for the calculation of sensitivity kernels for global seismology (Dahlen et al. 2000; Hung et al. 2000).

The use of seismic arrays can reduce the size of the Fresnel zone. In Fig. 4 we show an example for using a single station for the migration of a *PP* underside reflection. The details of the migration method will be explained in Sect. 5.1. Underside reflections of a discontinuity form a Fresnel zone that has a saddle-shaped form and regions up to several thousand of kilometers away from the theoretical reflection point can add to the observed signal (Neele et al. 1997; Zhao and Chevrot 2003; Schmerr and Garnero 2006). Figure 4 shows the Fresnel zone of a *PP* underside reflection from the global discontinuity at a depth of 410 km and two cross sections through a 3D volume of a time-migration essentially showing the Fresnel volume (Fig. 4b). Note the upward sloping of the isochrons along the great circle path and the downward slope perpendicular to the great circle path, indicating the min–max nature of *PP*. By using several stations of the array simultaneously the Fresnel zone size is strongly reduced since essentially only the Fresnel zone area common to all receivers contributes to the "array Fresnel" zone, therefore giving much better lateral resolution of the seismic data. The effect of the array processing on the

Fresnel volume (or smearing along an isochron) as shown in Figure 4b is similar in reducing the size of the Fresnel volume. The data for this example are synthetic seismograms with a dominant period of 2 s. Longer periods will increase both the Fresnel zone and the smearing of energy along the isochrons, but the effect of the array processing will be similar until the wavelength becomes too large and the used stations no longer work as an array.

4 Improving Seismic Resolution

The data example in Fig. 4 shows one method that helps to increase lateral resolution of seismic data—migration of array data. The migration technique is a technique often used in exploration seismology to obtain a clearer picture of the underground from the seismic data by collapsing diffractions to their origin and moving dipping reflectors into their true position. In the past, migration did not find much use in global seismology studies due to a lack of source receiver combinations that sample the underground structure densely enough for a successful application of migration. Owing to the proliferation of dense broadband networks and arrays on several continents more source-receiver geometries will be available for this kind of processing in the future.

4.1 Principles of Migration

The seismic wavefield contains energy due to refracted and reflected phases producing sharp arrivals in the seismogram. A seismogram only containing these arrivals would show only sharp arrivals with ray-theoretical travel times with little or no coda or source generated noise. Recorded seismograms look quite different than this idealistic picture and contain extensive codas (Rost et al. 2006) and energy that cannot be explained by wave propagation through radial Earth models. Much of this energy are diffractions and scattered arrivals from small-scale heterogeneities (i.e., velocity and/or density fluctuations of the Earth's material or diffractions due to corners and edges of reflecting surfaces). In exploration seismics, migration is generally used to move diffractions in common midpoint stacked reflection data back to their origin (Sheriff and Geldart 1995), therefore creating a better representation of the underground structure. Additionally, migration is used to find true reflection points in the case of dipping reflectors and to decrease the size of the Fresnel zone (Sheriff and Geldart 1995) as shown in Sect. 4.2. In global seismology migration has been used to detect small scatterers or reflectors from low amplitude arrivals in the seismic wavefield, e.g., (Thomas et al. 1999; Braña and Helffrich 2004; Revenaugh 1995a; Hutko et al. 2006; Kito et al. 2007a, b; Lynnes and Lay 1989; Scherbaum et al. 1997; Bostock and Rondenay 1999; Bank and Bostock 2003; Bostock 2003; Frederiksen and Revenaugh 2004). Many different techniques have been applied to many different tectonic settings to resolve Earth structure using scattered arrivals (e.g., see special volume edited by Dmowska (2008). Migration is also important if the assumption of plane waves arriving at the array breaks down (Thomas et al. 1999).

Migration in an exploration environment tends to move (migrate) reflection events to their original location (Gray et al. 2001) by calculating travel times in a velocity model. Several methods to calculate the traveltimes are used and include approximations to solve the wave equation (Claerbout and Doherty 1972), Kirchhoff migration (Schneider 1978), frequency-wavenumber migration (Gazdag 1978) and others (e.g. Baysal et al. 1983; McMechan 1983; Gray et al. 2001). The traveltimes are then used to remove migration

(a) 1 station / 9 stations (KNET configuration)

(b) perp gcp / along gcp
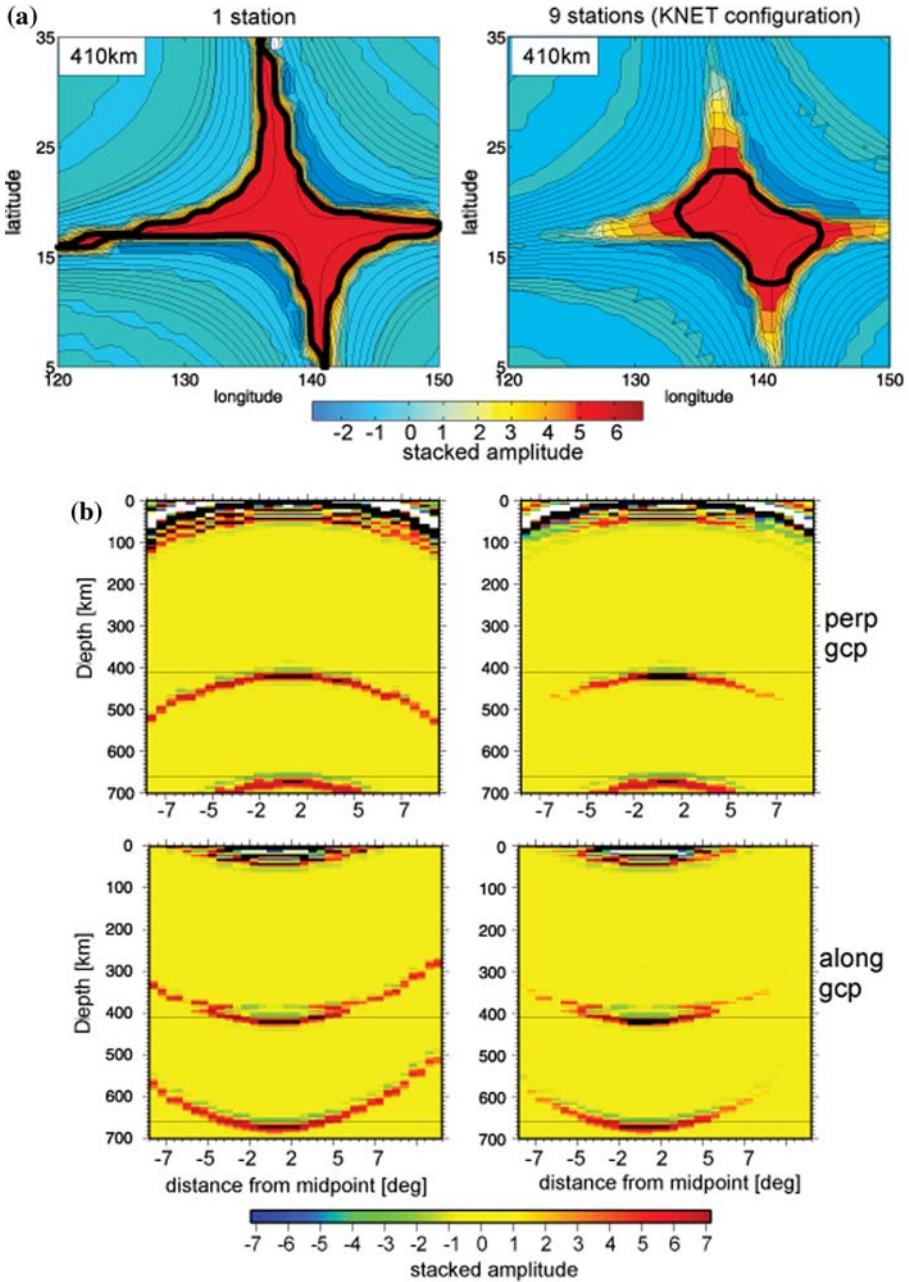
effects due to diffraction (i.e., along the diffraction hyperbola) from the data. The fast increase of high quality stations recording the elastic teleseismic wavefield in many regions of the Earth allows the adaptation or exploration methods requiring a very dense sampling of the seismic wavefield (e.g., the generalized Radon transform see e.g., Ma et al. (2007); Wang et al. (2006)).

◀**Fig. 4** Example of the effect of an array migration on the Fresnel zone for synthetic data calculated with the reflectivity method (Müller 1985) using the 1D Earth model IASP91 (Kennett and Engdahl 1991). **a** Fresnel zone for a *PP* underside reflection from the 410 km discontinuity. Note the saddle shaped form of the Fresnel zone (due to the min–max character of the *PP* wave) which allows contributions to the reflection from regions far away from the ray theoretical mid reflection point. The Fresnel zone as seen by a single station is shown on the *left*, while the Fresnel zone for a 9-element array [in a configuration as the Kyrgyz network KNET (Vernon 1994)] is shown to the *right*. Due to the array processing the Fresnel zone is strongly reduced in size, since only the Fresnel zone area that is common to all stations contributes to the array Fresnel zone. The direction along the great circle path is from the bottom right (latitude 5°N and longitude 150° E) to the top left (latitude 35°N and longitude 125° E) of the figures. **b** Migration example using 1 station (*left*) and 9 stations (*right*) of the underside reflected energy. Similar to the horizontal slice through the Fresnel volume these vertical cross sections perpendicular and along the great circle path show how using several station simultaneously decreases the Fresnel volume and the smearing along an isochron. Note the energy arriving from a reflection from the 410-km and 670-km discontinuity. In the case of only one station, stacked energy is the energy of the seismic energy measure at a single station

It is important to realize that the knowledge of the velocities is crucial for a successful migration, which can be a problem of migrating seismic data for the resolution of deep Earth structures. Another problem in most global migration methods is that only single scattering is assumed, which may lead to mis-positioning of scattered energy due to multiple scattering.

4.2 Simplified Time Migration

Global migration methods generally use array or network data for migration. Traveltimes for an appropriate Earth model are calculated for a three-dimensional grid around a target zone and raytracing is used to calculate traveltimes forward from one or multiple sources to each grid point and backward from each grid point to each receiver (Fig. 5a). These traveltimes are then used to shift the traces of the individual stations of the network or array to account for theoretical traveltimes of energy originating (scattering or reflecting) at each grid point and subsequently all recordings are summed or stacked. Measuring the amplitude or energy of stacked traces in a time window around a potential target phase originating from this grid point allows an estimate of the energy arriving from each grid point (Fig. 5a). The amplitude or energy is then stored in the 3D grid and regions with large stacked amplitudes indicate regions of scattering or reflection (Fig. 5b) (Thomas et al. 2004). Two cross sections through the 3D volume of stacked energy for each grid point are shown in Fig. 5b, one along the great circle path and the cross section perpendicular to the great circle path. The reflection at the core-mantle boundary (CMB) and a reflection at the D″ discontinuity, which was added to the 1D Earth model IASP91 (Kennett and Engdahl 1991), can be clearly identified as areas of large stacked migration amplitudes. In some cases the use of amplitude-depth profiles showing maximum amplitudes in each layer along a 1D vertical profile through the 3D volume can simplify the detection of reflectors and the measurement of accurate reflector depths (Kito et al. 2007b; Thomas and Billen 2009). Amplitude depth profiles are generated by measuring the absolute amplitude at the theoretical reflection point at each layer and displaying it over depth. Amplitude depth profiles can also be generated by taking into account the Fresnel zone where the maximum amplitude in the Fresnel zone around the ray is detected. This allows the detection of out-of-plane arrivals.
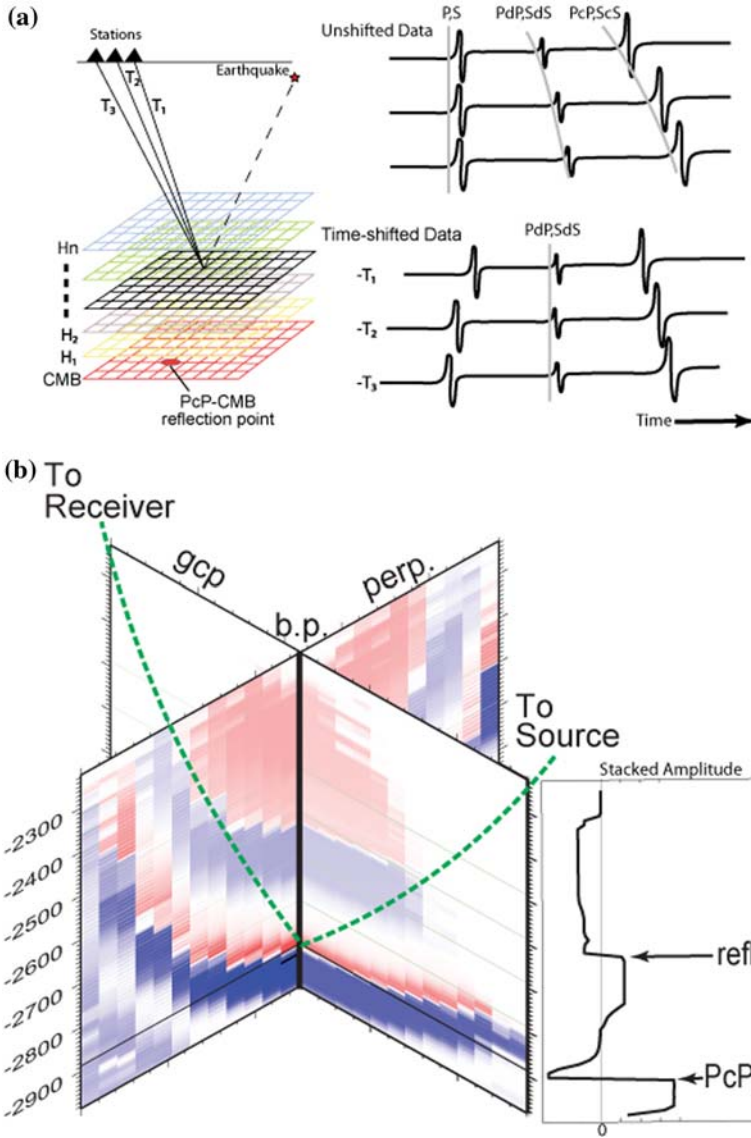
Fig. 5 Sketch explaining migration. For virtual grids within a volume in the deep Earth traveltimes from seismic source(s) to each grid point and from each grid point to each station are calculated for a velocity Earth model (T_1, T_2, T_3). The source-grid-receiver travel times define the shift time to be applied to the recordings to simulate energy originating from a grid point within the study volume. If a certain arrival indeed originates from this point the recordings from the array align and sum up coherently (*right*). The separation of the depth layers (H_1, ..., H_n) is chosen appropriately. **b** Cross sections through the migration volume of synthetic data calculated with the reflectivity method and the model PWDK (Weber and Davis 1990) showing the isochrones for *PcP* and a reflection (*PdP*) from the D″ discontinuity in this depth migrated (assuming a 1D Earth model) section. The cross sections are parallel and perpendicular to the great circle path with the ray theoretical *PcP* CMB reflection point in the center. Also shown is the amplitude depth profile, a measurement of the stacked amplitude at the theoretical reflection point for each depth, which simplifies the depth detection of the reflector

4.3 Kirchhoff Migration or Diffraction Stacking

Kirchhoff or diffraction migration is based on Huygens principle which states that any point of a wavefront at time t_1 acts as a secondary source and the resulting wavefront at time t_2 is the superposition of all contributions of these secondary sources. For any reflection this means that the reflection can be replaced theoretically through secondary sources along the reflector, i.e., by closely spaced diffraction points. Each of the diffraction points produces a diffraction hyperbola, whose curvature depends on the velocity structure (Fig. 6). The superposition of the diffraction hyperbolae and the mislocation of reflection points for dipping surfaces leads to an incorrect image of the subsurface. This type of migration is widely used in reflection seismic processing (Bednar 2005) and finds more and more application in global seismology.
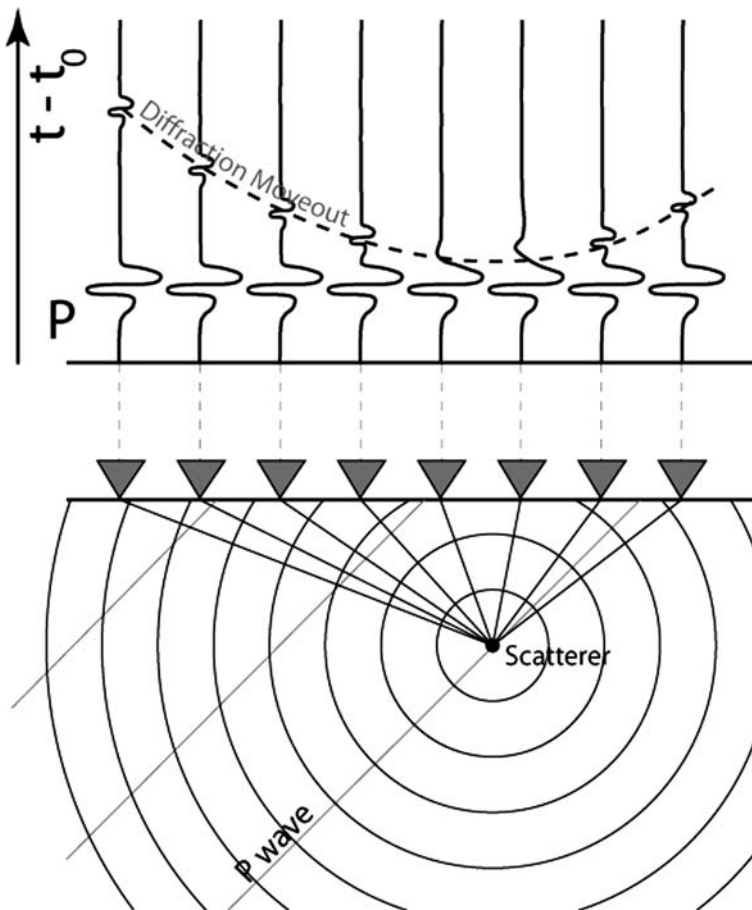
Fig. 6 Sketch of diffraction stacking for a scattering source close to the receivers (*triangles*). Each point of the underground can be considered as a secondary source producing diffracted arrivals. Stacking the array recordings along diffraction curves (i.e., considering the different move out of the "scattered" energy relative to the reference arrival) can be used to migrate back the energy to its origin. After Revenaugh (1995a)

In global seismology the 3D diffraction hyperbolas through a generally 1D Earth model must be calculated and the seismic traces are summed or stacked along these hyperbolas (Hutko et al. 2006). The method assumes that any point within the study volume acts as point scatterer and the final image of the structure in the seismic wavefield is the superposition of the contributions from these scatterers. One simplification is to assume isotropic point scattering only (Revenaugh 1995a, b). If $x_{ij}(t_k)$ is the time series recorded at the jth station of the ith source [with $t_k = t_0 + k\Delta t$, Δt being the sampling interval and k a digital sample number, i.e., time is referenced to a canonical start time t_0 (Revenaugh 1995a)] we can calculate the travel time from a source i at position s_i scattered at position q and recorded at station j at position r_j as (Revenaugh 1995a):

$$\tau_{ij}(q) = t_0 + T(s_i, q) + T(q, r_j) - T(s_i, r_j) \tag{13}$$

with $T(a,b)$ being the traveltimes between points a and b (i.e., $T(s_i, q)$ is the traveltime from the source at s_i to the scatterer at location q and $T(q, r_j)$ is the traveltime from the scatterer to the receiver at r_j). The migration value at q, $S(q)$, can be calculated through (Revenaugh 1995a):

$$S^n(q) = \frac{1}{K(q)} \sum_{i=1}^{N} \sum_{j=1}^{M} \sum_{k=1}^{k_{max}} \left\{ X_j(q) W \left[\tau_{ij}(q), T(q, r_j) \right] \sum_l \left| x_{ij}(t_k - l\Delta t) \right| \right\}^{1/n} \tag{14}$$

with k_{max} the number of recorded samples beyond t_0, and N and M the number of sources and receivers, respectively. $W[\tau_{ij}(q), T(q, r_j)]$ and $X_j(q)$ being windowing operators over time and distance, respectively, that have to contain corrections for geometric spreading, and receiver terms. $K(q)$ is a normalizing factor to equal the sums of all weights. The n indicates n-th root stacking (McFadden et al. 1986) with $n = 1$ indicating a linear stack. Equation 14 represents a summation of many different sources and receivers along traveltime surfaces and likely sources of scattering are indicated by large values of $S(q)$. Using a combination of different sources and receivers requires careful receiver and source deconvolution which can introduce sidelobes that can be misinterpreted as additional arrivals. Since the travel times are calculated for specific velocity models a detailed knowledge of the full velocity structure within the study region is required to obtain correct images of the underground.

4.4 Slowness-Backazimuth Weighted Migration

The Kirchhoff migration described in Sect. 5.3 essentially introduces a weighting of the traces based on the traveltimes. Other or additional weighting factors are feasible and the controlled-source seismic community applies e.g., weighting factors based on the incidence angle of the energy (Takahashi 1995; Bellefleur et al. 2004; Luth et al. 2005). Kito et al. (2007a) extended this principle to use earthquake sources to study the Earth's deep interior. They apply a weighting factor for slowness and backazimuth with lower weighting applied to energy originating from gridpoints which will lead to strong slowness and backazimuth deviations from theoretical values (in general calculated for 1D Earth models). The weighting for energy arriving from a position q with observed slowness (backazimuth) u_{obs} (θ_{obs}) and theoretical slowness (backazimuth) u_{theo} (θ_{theo}) within the sampling volume is defined as

$$W_{\text{slow}}(\boldsymbol{q}) = F\left[\frac{u_{\text{obs}}(\boldsymbol{q}) - u_{\text{theo}}(\boldsymbol{q})}{u_{\text{dev}}^{\text{max}} - u_{\text{theo}}(\boldsymbol{q})}\right] \tag{15}$$

$$W_{\text{baz}}(\boldsymbol{q}) = F\left[\frac{\theta_{\text{obs}}(\boldsymbol{q}) - \theta_{\text{theo}}(\boldsymbol{q})}{\theta_{\text{dev}}^{\text{max}} - \theta_{\text{theo}}(\boldsymbol{q})}\right] \tag{16}$$

for slowness (u) and backazimuth (θ), respectively. F can be an arbitrary function defining the weighting, e.g., a Gaussian (Kito et al. 2007a), but other weighting functions are possible. $u_{\text{dev}}^{\text{max}}$ and $\theta_{\text{dev}}^{\text{max}}$ are the maximum slowness and backazimuth deviations within the study volume, respectively.

Similar to Eq. 14 the weighting can be enhanced by applying a power of n, e.g., to focus on energy arriving within the first Fresnel volume.

$$S_{\text{w}}(t, \boldsymbol{q}) = S(t, \boldsymbol{q}) \cdot [W_{\text{slow}}(\boldsymbol{q})]^n \cdot [W_{\text{baz}}(\boldsymbol{q})]^n \quad (n = 1, 2, \ldots) \tag{17}$$

with $S(t,\boldsymbol{q})$ and $S_w(t,\boldsymbol{q})$ being the unweighted and weighted stack as a function of time (t) of the data for a location $\boldsymbol{q}$, respectively.

The slowness-backazimuth weighting of the migrated data leads to increased resolution, smaller Fresnel zones and a generally sharper image of potential scattering locations (Kito et al. 2007a).

Kito et al. (2007a) use only a single event for the weighted migration, so essentially a receiver array migration. Nonetheless, the method can equally well be applied to a combination of source and receiver arrays, although the application to a single source avoids complication due to source deconvolution.

5 Resolution of Deep Earth Structure

This section gives some data examples how array analysis of seismic data can help to improve resolution. We will also introduce further issues of seismic resolution and dangers in using some methods without further investigation of the wavefield.

5.1 Scattering

The ability of arrays to detect and locate energy traveling along paths not predicted by ray tracing through 1D Earth models, i.e., traveling off the great circle path connecting source and receiver can be employed to resolve the fine scale structure of the deep Earth. Arrays have extensively been used to detect and locate small-scale heterogeneities in the Earth that produce scattered energy (Revenaugh 1995a, b; Thomas et al. 1999; Braña and Helffrich 2004; Hutko et al. 2006; Kaneshima and Helffrich 1998; Castle and van der Hilst 2003; Rost et al. 2008; Kito et al. 2003, 2008 and others). Some of these methods, going back to different migration schemes, have been described in Sect. 5.

Even without using migration methods, arrays can be used to detect this off-gcp energy by "steering" the array towards the off-gcp directions, i.e., without restricting the detection capabilities to the gcp. Several methods allowing this have been developed in the past and have been described briefly in Sect. 3 or elsewhere (Harjes and Henger 1973; Rost and Thomas 2002; Schweitzer et al. 2002).

Scattered phases are important in resolving Earth structure since they can give constraints on material properties (i.e., velocity and density variations due to e.g., chemical heterogeneities) below the seismic wavelength—a wavelength range that is inaccessible to other seismic methods. Scattering has been detected throughout the Earth from crust to core (Revenaugh 1995a, b; Hedlin and Shearer 2000, 2002; Earle and Shearer 1998, 2001; Vidale and Earle 2000; Doornbos 1974; Tkalčić et al. 2006). Several phases showing scattering have been used with those maximum travel time phases (such as *PKP*, *PKKP*, *P'P'* and *PP* i.e., underside reflection type phases) being favoured due to the fact that scattering from the deep Earth in general arrives before the main arrival, making the separation of the scattered energy from other coda effects such as *P*-to-*S* conversions close to the station easier. Figure 7a, b show a stack using beampacking of a 100 s time window appropriate to detect *PKKP* scattering from the CMB reflection point (Earle 2002) (*PK•KP*—Fig. 7c, d). Figure 7a uses a rotated slowness coordinate system where the East–West and North–South slownesses are rotated into radial (u_r) and transverse (u_t) slowness using the backazimuth of the great circle path. Using radial and transverse slowness makes the off gcp arrival of the scattered energy obvious since we expect energy traveling along the great circle path to arrive with zero transverse slowness (Earle 2002). Beampacking calculates array beams for a wide combination of slowness and backazimuth values in the time domain and measures maximum beam amplitude in a time window of interest. The stacking in the time domain is slower than the frequency domain *fk*-analysis (Capon 1969) but gives similar results with high stack amplitudes for specific slowness and backazimuths indicating the direction of incidence for the energy in the time window. The beampower displays in Fig. 7a, b clearly show the incoming energy (high energy indicated by hot colors) from off-gcp as expected for *PK•KP* (both in Fig. 7a) in radial and transverse slowness range as well as in Fig. 7b in slowness backazimuth space (gcp indicated by dashed line). The display also shows the effect of the YKA array configuration (cross shaped ARF) with the overlapping of two responses of the array to two scatterer locations at the CMB. The slowness shifted shapes of the ARF can clearly be identified, but care must be taken to not interpret the sidelobes of the ARF as actual arriving energy. Standard array processing focusing on energy traveling along the gcp suppresses this energy or would map it to incorrect slowness values (Rost and Thomas 2002).

Using the slowness and backazimuth information from this analysis allows a location of the scattering regions at the core-mantle boundary by back tracing the energy to the CMB using the directivity information. Using an array with a sharper array response function (i.e., less sidelobes) would allow a better localization of the scattering area [e.g., LASA (Earle and Shearer 1998)]. This *PKKP* scattering example and other scattering examples show that much information can be gained from seismic energy not traveling along paths predicted by ray-tracing methods and this information should be used to resolve Earth structure.

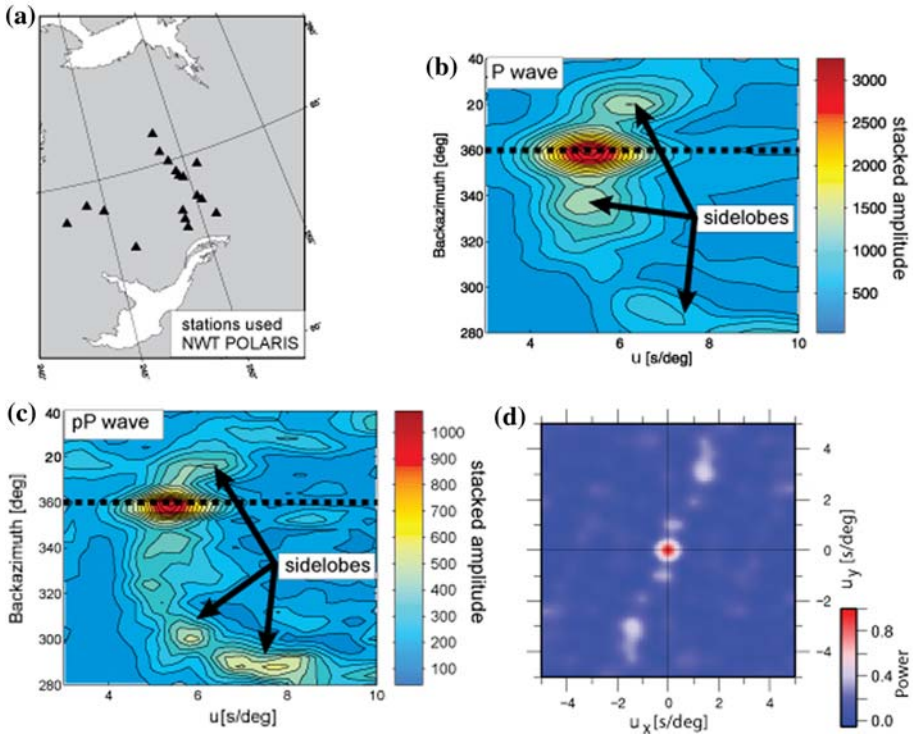5.2 Slowness-Backazimuth Stacking

The second example shows the case of searching for out-of-plane waves that have been reflected at the Aleutian subduction zone. Several previous studies have investigated out-of-plane reflections [e.g., (Weber and Wicks 1996; Kaneshima and Helffrich 1999; Rost et al. 2008; Kito et al. 2008)] and in several cases slowness-backazimuth stacking or *fk*-analyzes have been used.

This example shows data from the Hindu Kush area recorded at the North West Territories installation of the Canadian POLARIS consortium (POLARIS-NWT) (Fig. 8a).
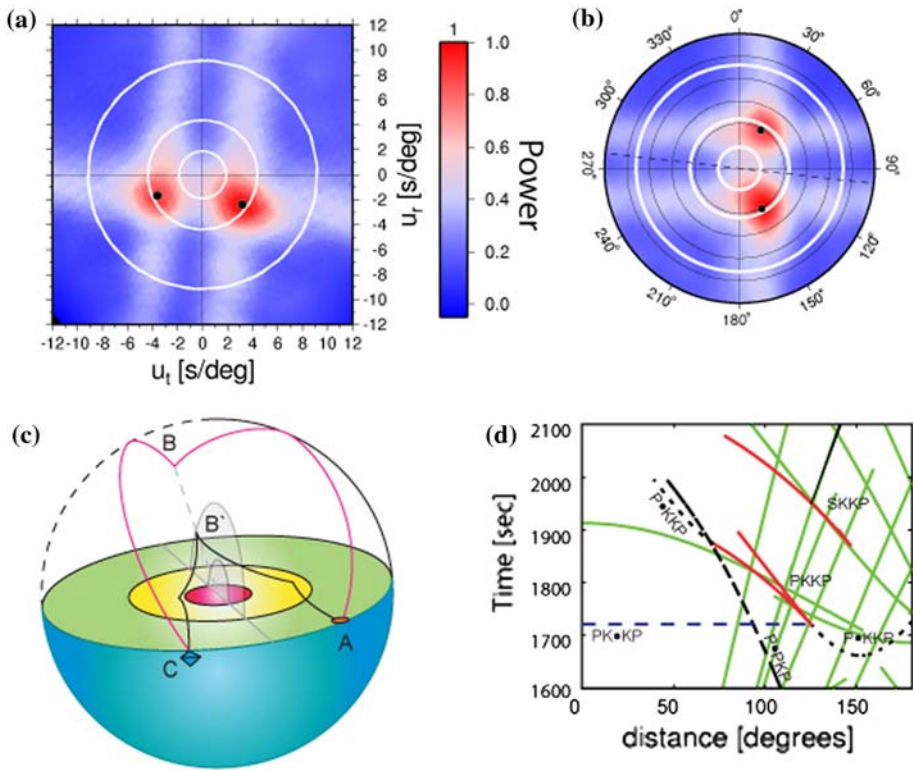
Fig. 7 Time-domain beampacking example of an event on 28 January 1999, 08:10 recorded at YKA. For the beampack, array beams for all combinations in slowness and backazimuth are calculated and maximum beam amplitudes in a 100 s long time window that has been identified as the *PKKP* scattering time window (Earle 2002) are measured. **a** Beam power in transverse and radial slowness space, where the original slowness and backazimuth are rotated into the radial and transverse directions, i.e., transverse slowness values of 0 indicate energy traveling along the great circle path. *White lines* indicate theoretical slownesses of 1.9, 4.4, and 9.2 s/deg, i.e., inner core boundary, core mantle boundary and crustal slownesses, respectively. The *two red beam* maxima indicate *PKKP* energy scattered at the CMB (i.e., slownesses around 4.4 s/deg) from two points roughly symmetrically off gcp. The maximum beam power in the stacks is indicated by black circles. **b** Same as (**a**) but in the traditional backazimuth-slowness display. The *dashed line* indicates the gcp backazimuth showing the energy traveling off gcp. **c** Principle of off-gcp *PKKP* underside CMB scattering (*PK•KP*) (after Chang and Cleary 1981). The plane through AC marks the gcp plane, while *PKKP* scattering happens at B′ with a surface projection of B clearly off gcp. **d** Theoretical travel times of different *PKKP* scattering schemes (Earle 2002) with *PK•KP* being the scattering off the CMB underside scattering shown in (**a** and **b**). Note that the minimum traveltime of *PK•KP* as determined by raytracing shows a constant travel time independent of distance (Earle 2002) The *red lines* are the major phases *PKKP* and *SKKP* while *green lines* are traveltime curves of other body waves (*S, S*diff*, SP, SPP, PP, PPP, PPPP, PcPPKP and PKJKP*) in the same time window calculated for the IASP91 velocity model (Kennett and Engdahl 1991). Minimum traveltimes for the scattered waves are shown as *dashed lines*

The slowness-backazimuth plot of the *P*-wave (Fig 8b) shows a strong maximum at the theoretical backazimuth of 360°, indicated by the dashed horizontal line. The slowness of the data is the expected theoretical slowness from 1D Earth models for a *P*-wave at this distance (around 79°). In addition to the strong maximum, sidelobes are visible, that are due to the configuration of the POLARIS-NWT array (Array response function in Fig. 8d).

Fig. 8 a Station configuration of the POLARIS NWT installation in northern Canada. Stations are indicated by *triangles*. **b** Slowness-Backazimuth stacks of a 5 s time window around the *P*-arrivals of an earthquake in the Hindukush region. The *P*-wave arrival can be detected as the strong arrival with a backazimuth of 360°. Additional energy with deviating backazimuth and slowness values is likely not due to actual additional seismic energy, but due to sidelobes within the response function of the POLARIS installation. **c** Same as (**b**) but for a 5 s time window around the *pP* arrival. The side lobes here are more pronounced than in (**a**). **d** Array Response Function of the stations in (**a**) calculated for a 8 s wavelet. Note the sidelobes in *NEN* and *SWS* directions (approximate towards 20 and 200°). These sidelobes generate the energy arriving off-gcp in (**b**, **c**)

These sidelobes extend to slowness and backazimuth values that are considerably different from the expected values. These sidelobes are not out-of-plane reflections (as shown in 6.1) since here only the time window around the *P*-wave (5 s window width) was used for the slowness-backazimuth plot and no dominant coherent coda energy can be observed in the data. These ARF sidelobes make the search for out-of-plane reflections difficult since great care has to be taken not to identify the sidelobes as an interpretable signal.

The ARF shows several maxima (Fig. 8d) which can be translated into the slowness (u) and backazimuth (θ) of the slowness-backazimuth plot using:

$$u = \sqrt{u_x^2 + u_y^2}$$
$$\theta = a\tan\left(\frac{u_x}{u_y}\right) \tag{18}$$

Using the first sidelobes of the ARF (Fig. 8d) the energy in Fig. 8b, c can be easily explained. The stronger sidelobes with about 3 s/deg deviation actually will plot outside of the slowness backazimuth region shown in Fig. 8b.

Figure 8c shows a slowness-backazimuth plot of the same event 50 s after the first *P* arrival showing the *pP* time window. In this example, the energy in the sidelobes is more pronounced than in the *P*-wave time window but the distribution of energy is very similar to the *P*-wave example and includes energy from a depth phase of *P* with the correct slowness and backazimuth (indicated by the dashed line). In this case it would lead to misinterpretations to attribute the energy arriving with slowness 7.7 s/deg and backazimuth of 290° to an off-gcp reflection, even though it would be the correct slowness and backazimuth for a reflection from the Aleutian area.

These examples show that it is very important to take the receiver characteristics of any array or network into account when analyzing subtle energy that travels out of the source receiver plane. Mislocation of scattered energy due to the misinterpretation of energy due to aliasing from the ARF for arbitrary network configurations without careful control of the ARF can easily bias the interpretation.

5.3 Migration of Upper Mantle Transition Zone Reflectors

In our third example, a simplified time migration method is used to search for upper mantle reflectors in the transition zone. This example shows recordings from the Kyrgyz network KNET (Vernon 1994) and the temporary GHENGIS array (Roecker 2001) of an event in the Tonga subduction zone. Targets of this study are upper mantle reflectors between 0 and 800 km depth with *P*-waves that sample the South West Pacific (Thomas and Billen 2009). Figure 9a shows the traces aligned on the *PP* wave arrival, a *P*-wave once reflected at the surface midway between source and receiver, with obvious energy arriving ahead of *PP*. Some of these phases exhibit different move-out compared to *PP* and are therefore unlikely to be *PP* precursors, but likely top side reflections off discontinuities (Schmerr and Garnero 2006) or scattered energy (Rost et al. 2008).

When applying the migration method (Fig. 9b), the min-max character and typical saddle shape of the *PP*-wave Fresnel zone can be observed. The isochrons of *PP* and subsequently the precursors extend far away into the mantle. Note again, the upward sloping of the isochrons along the great circle path and the downward slope perpendicular to the great circle path, due to the min–max nature of *PP* (see also Fig. 4b). In Fig. 9b the arrival of $P^{410}P$ can clearly be identified as energy focusing at a migration depth of approximately 420 km. The *PP* energy focuses at the surface due to the *PP* alignment of the recordings, therefore, the measured depth of the precursor is dependent on the applied velocity model. The energy of the shifted and stacked traces is largest in this case near the theoretical reflection point but out-of-plane reflections can be detected by using the complete Fresnel zone (as shown in Fig. 4) and searching for the maximum energy within the 1 s isochrons. To reduce the reflected energy that arrives out of plane (i.e., along the isochrons) stacking with backazimuth weighting (Kito et al. 2007a, b) will increase the resolution. In this example, the broadband recordings have been filtered with a 5 s lowpass filter and the central part of the 1D Fresnel zone (with a *T/4* criterion, *T* being the period of the wave) therefore has approximate dimensions of 165 by 500 km.

This example also shows the danger in using migration for out-of-plane reflections in that energy spreads along an isochron, which could lead to misinterpretation. Energy that is
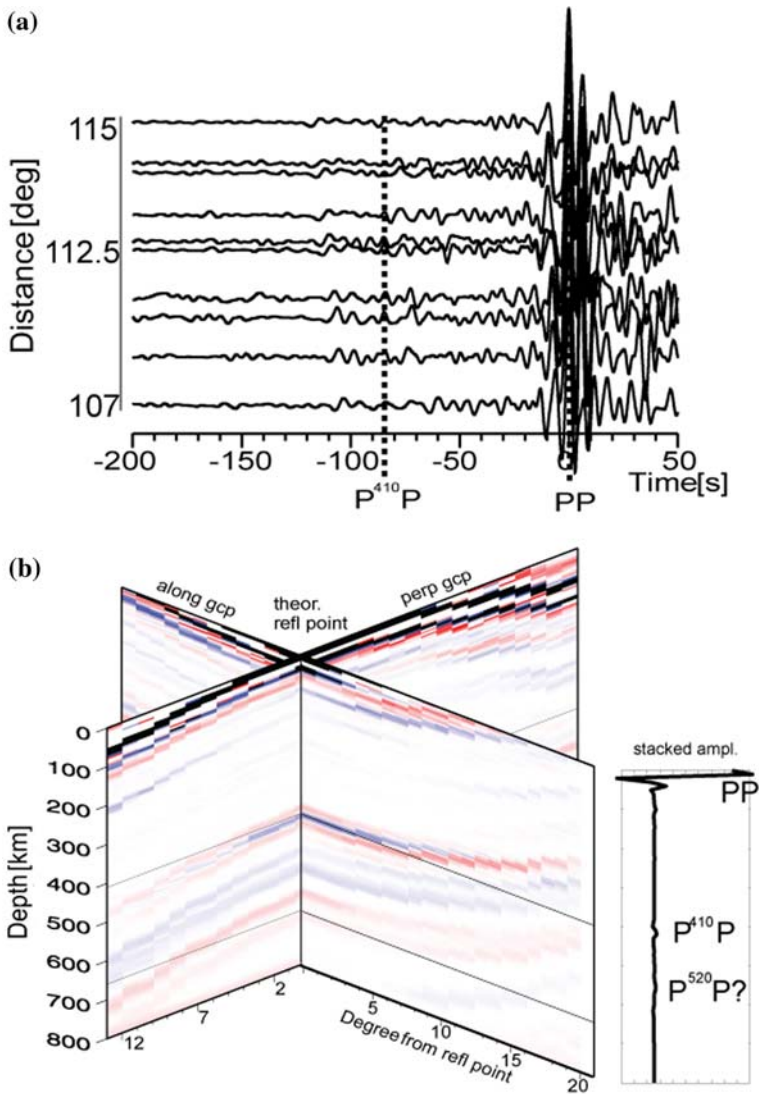
Fig. 9 a Seismic data including the *PP* wave and its precursors recorded at the KNET and GHENGIS networks in central Asia. The data have been filtered with a 5 s lowpass and are aligned on the *PP* arrival. The theoretical arrival time of the 410-km underside reflection $P^{410}P$ has been marked. The seismic traces have been sorted according to distance. **b** Migrated seismic data. Two cross-sections (perpendicular and parallel to the great circle path) are shown with *red* and *blue* colors indicating positive and negative amplitudes within the stack, respectively. Also shown is an amplitude-depth profile, taken vertically beneath the theoretical reflection point of *PP*, showing the *PP* and $P^{410}P$ arrivals

arriving parallel to the observed smearing of energy from the *PP* wave along an isochron should therefore be analyzed with other methods such as *fk*-analysis, to establish its potential out-of-plane character.

6 Conclusions

The use of arrays offers several advantages over employing single stations. With their ability to sample the seismic wavefield in three-dimensions much more information can be gained and used to study the Earth. Precise source location is also possible through specially designed arrays. With the growing number of networks with reasonable timing accuracy and high station densities array methods will be applied more often and new methods can be adopted from the industrial exploration seismology community due to the higher sampling of the seismic wavefield.

Conventional seismic array methods based on shifting and stacking data, such as beamforming and vespagrams or simultaneous determination of slowness and backazimuth provide estimates of the angle of incidence at an array. This in turn provides the possibility to find the 'origin' of a seismic wave and its travel path, although there are some ambiguities in doing this (e.g., P at 40° will map in the same slowness space as PP from a source 80° away). The Fresnel zone is usually seen as a limit to resolution and we show how the use of seismic arrays can decrease the Fresnel zone as well as smearing along isochrons.

Migration methods used in teleseismic studies provide a useful tool to increase the resolution of seismic structures in the deep Earth, especially combined with using broadband arrays, where different frequency bands can be used. Extensions to the migration, such as slowness-backazimuth or travel time weighting further improve the resolution.

These new developments in parallel with an increasing number of international network deployments (both temporary and permanent) and the good availability of data through national and international data centers will allow us a much better sampling and better resolution of the interior of our planet.

References

Avants M, Lay T, Russell S, Garnero E (2006) Shear velocity variation within the D″region beneath the central Pacific. J Geophys Res 111:B05305. doi:10.1029/2004JB003270

Bank C, Bostock M (2003) Linearized inverse scattering of teleseismic waves for anisotropic crust and mantle structure: 2. Numerical examples and application to data from Canadian stations. J Geophys Res 108(B5):2259. doi:10.1029/2002JB001951

Bastow I, Stuart G, Kendall J, Ebinger C (2005) Upper-mantle seismic structure in a region of incipient continental breakup: northern Ethiopian rift. Geophys J Int 162:479–493. doi:10.1111/j.1365-246X.2005.02666.x

Baysal E, Kosloff D, Sherwood J (1983) Reverse time migration. Geophysics 48:1514–1524. doi:10.1190/1.1441434

Bednar J (2005) A brief history of seismic migration. Geophysics 70:3MJ–20MJ

Bellefleur G, Muller C, Snyder D, Matthews L (2004) Downhole seismic imaging of a massive sulfide orebody with mode-converted waves, Halfmile Lake, New Brunswick, Canada. Geophysics 69:318–329. doi:10.1190/1.1707051

Bondar I, North R, Beall G (1999) Teleseismic slowness-azimuth station corrections for the international monitoring system seismic network. Bull Seismol Soc Am 89:989–1003

Bostock M (2003) Linearized inverse scattering of teleseismic waves for anisotropic crust and mantle structure: 1. Theory. J Geophys Res 108(B5):2258. doi:10.1029/2002JB001950

Bostock M, Rondenay S (1999) Migration of scattered teleseismic body waves. Geophys J Int 137:732–746. doi:10.1046/j.1365-246x.1999.00813.x

Bracewell RN (1965) The Fourier transform and its applications, 3rd edn. McGraw-Hill, New York

Braña L, Helffrich G (2004) A scattering region near the core-mantle boundary under the North Atlantic. Geophys J Int 158:625–636. doi:10.1111/j.1365-246X.2004.02306.x

Capon J (1969) High resolution frequency-wavenumber spectrum analysis. Proc IEEE 57:1408–1428. doi:10.1109/PROC.1969.7278

Carpenter E (1965) A historical review of seismometer array development. Proc IEEE 53:1816–1821. doi:10.1109/PROC.1965.4452

Castle J, van der Hilst R (2003) Searching for seismic scattering off mantle interfaces between 800 and 2000 km depth. J Geophys Res 108(B2):2095. doi:10.1029/2001JB000286

Cerveny V, Soares J (1992) Fresnel volume ray tracing. Geophysics 57:902–915. doi:10.1190/1.1443303

Chang A, Cleary J (1981) Scattered PKKP—further evidence for scattering at a rough core-mantle boundary. Phys Earth Planet Inter 24:15–29. doi:10.1016/0031-9201(81)90075-3

Claerbout J, Doherty S (1972) Downward continuation of moveout corrected seismograms. Geophysics 37:741–768. doi:10.1190/1.1440298

Clouser R, Langston C (1995) Modeling *P*-Rg conversions from isolated topographic features near the NORESS array. Bull Seismol Soc Am 85:859–873

Dahlen F, Hung S, Nolet G (2000) Frechet kernels for finite-frequency traveltimes—I. Theory. Geophys J Int 141:157–174. doi:10.1046/j.1365-246X.2000.00070.x

Davies D, Kelly E, Filson J (1971) VESPA process for analysis of seismic signals. Nat Phys Sci (Lond) 232:8–13

Dmowska R (2008) Earth heterogeneity and scattering effects on seismic waves. Adv Geophys 50:1–476. doi:10.1016/S0065-2687(08)00001-0

Doornbos D (1974) Seismic-wave scattering near caustics—observations of PKKP precursors. Nature 247:352–353. doi:10.1038/247352a0

Earle P (2002) Origins of high-frequency scattered waves near PKKP from large aperture seismic array data. Bull Seismol Soc Am 92:751–760. doi:10.1785/0120010169

Earle P, Shearer P (1998) Observations of high-frequency scattered energy associated with the core phase PKKP. Geophys Res Lett 25:405–408. doi:10.1029/97GL53365

Earle P, Shearer P (2001) Distribution of fine-scale mantle heterogeneity from observations of *P*-diff coda. Bull Seismol Soc Am 91:1875–1881. doi:10.1785/0120000285

Eaton D, Stewart R, Harrison M (1991) The Fresnel zone for *P*-SV waves. Geophysics 56:360–364. doi:10.1190/1.1443050

Frederiksen A, Revenaugh J (2004) Lithospheric imaging via teleseismic scattering tomography. Geophys J Int 159:978–990. doi:10.1111/j.1365-246X.2004.02414.x

Friedrich A, Krüger F, Klinge K (1998) Ocean-generated microseismic noise located with the Grafenberg array. J Seismol 2:47–64. doi:10.1023/A:1009788904007

Gazdag J (1978) Wave-equation migration with phase-shift method. Geophysics 43:1342–1351. doi:10.1190/1.1440899

Gelchinsky B (1985) The formulae for the calculation of the Fresnel zones or volumes. J Geophys—Zeitschr Geophys 57:33–41

Gray S, Etgen J, Dellinger J, Whitmore D (2001) Seismic migration problems and solutions. Geophysics 66:1622–1640. doi:10.1190/1.1487107

Green P, Frosch R, Romney C (1965) Principles of an experimental large aperture seismic array (lasa). Proc IEEE 53:1821–1833. doi:10.1109/PROC.1965.4453

Hagedoorn JG (1954) A process of seismic reflection interpretation. Geophys Prospect 2:85–127. doi:10.1111/j.1365-2478.1954.tb01281.x

Harjes H (1990) Design and siting of a new regional array in central-Europe. Bull Seismol Soc Am 80:1801–1817

Harjes H, Henger M (1973) Array seismologie. Z Geophys 39:865–905

Haubrich R (1968) Array design. Bull Seismol Soc Am 58:977–991

Hedlin M, Shearer P (2000) An analysis of large-scale variations in small-scale mantle heterogeneity using Global Seismographic Network recordings of precursors to PKP. J Geophys Res 105:13655–13673. doi:10.1029/2000JB900019

Hedlin M, Shearer P (2002) Probing mid-mantle heterogeneity using PKP coda waves. Phys Earth Planet Inter 130:195–208. doi:10.1016/S0031-9201(02)00007-9

Henyey T (2000) Earthscope: a look into our continent. Geotimes 45:5

Hung S, Dahlen F, Nolet G (2000) Frechet kernels for finite-frequency traveltimes—II. Examples. Geophys J Int 141:175–203. doi:10.1046/j.1365-246X.2000.00072.x

Husen S, Kissling E (2001) Local earthquake tomography between rays and waves: fat ray tomography. Phys Earth Planet Inter 123:127–147. doi:10.1016/S0031-9201(00)00206-5

Hutko A, Lay T, Garnero E, Revenaugh J (2006) Seismic detection of folded, subducted lithosphere at the core-mantle boundary. Nature 441:333–336. doi:10.1038/nature04757

Johnson DH, Dudgeon DE (1992) Array signal processing: concepts and techniques. Simon & Schuster, New York

Kanasewich E, Hemmings C, Alpaslan T (1973) Nth root stack nonlinear multichannel filter. Geophysics 38:328–337. doi:10.1190/1.1440343

Kaneshima S, Helffrich G (1998) Detection of lower mantle scatterers northeast of the Marianna subduction zone using short-period array data. J Geophys Res 103:4825–4838. doi:10.1029/97JB02565

Kaneshima S, Helffrich G (1999) Dipping low-velocity layer in the mid-lower mantle: evidence for geo-chemical heterogeneity. Science 283:1888–1891. doi:10.1126/science.283.5409.1888

Kennett B, Engdahl E (1991) Traveltimes for global earthquake location and phase identification. Geophys J Int 105:429–465. doi:10.1111/j.1365-246X.1991.tb06724.x

King D, Husebye E, Haddon R (1976) Processing of seismic precursor data. Phys Earth Planet Inter 12: 128–134. doi:10.1016/0031-9201(76)90042-X

Kito T, Krüger F (2001) Heterogeneities in D″ beneath the southwestern Pacific inferred from scattered and reflected P-waves. Geophys Res Lett 28:2545–2548. doi:10.1029/2000GL012801

Kito T, Shibutani T, Hirahara K (2003) Scattering objects in the lower mantle beneath northeastern China observed with a short-period seismic array. Phys Earth Planet Inter 138:55–69. doi:10.1016/S0031-9201(03)00080-3

Kito T, Rietbrock A, Thomas C (2007a) Slowness-backazimuth weighted migration: a new array approach to a high-resolution image. Geophys J Int 169:1201–1209. doi:10.1111/j.1365-246X.2007.03379.x

Kito T, Rost S, Thomas C, Garnero E (2007b) New insights into the P- and S-wave velocity structure of the D″ discontinuity beneath the Cocos Plate. Geophys J Int 169:631–645. doi:10.1111/j.1365-246X.2007.03350.x

Kito T, Thomas C, Rietbrock A, Garnero E, Nippress SEJ, Heath AE (2008) Seismic evidence for a sharp lithospheric base persisting to the lowermost mantle beneath the Caribbean. Geophys J Int 174: 1019–1028. doi:10.1111/j.1365-246X.2008.03880.x

Knapp R (1991) Fresnel zones in the light of broad-band data. Geophysics 56:354–359. doi:10.1190/1.1443049

Krüger F, Weber M (1992) The effect of low-velocity sediments on the mislocation vectors of the GRF array. Geophys J Int 108:387–393. doi:10.1111/j.1365-246X.1992.tb00866.x

Krüger F, Weber M, Scherbaum F, Schlittenhardt J (1993) Double-beam analysis of anomalies in the core-mantle boundary region. Geophys Res Lett 20:1475–1478. doi:10.1029/93GL01311

Krüger F, Scherbaum F, Weber M, Schlittenhardt J (1996) Analysis of asymmetric multipathing with a generalization of the double-beam method. Bull Seismol Soc Am 86:737–749

Lay T, Hernlund J, Garnero E, Thorne M (2006) A post-perovskite lens and D″ heat flux beneath the central. Pac Sci 314:1272–1276

Luth S, Buske S, Giese R, Goertz A (2005) Fresnel volume migration of multicomponent data. Geophysics 70:S121–S129. doi:10.1190/1.2127114

Lynnes C, Lay T (1989) Inversion of P-Coda for isotropic scatterers at the Yucca Flat test site. Bull Seismol Soc Am 79:790–804

Ma P, Wang P, Tenorio L, de Hoop M, van der Hilst R (2007) Imaging of structure at and near the core-mantle boundary using a generalized radon transform: 2. Statistical inference of singularities. J Geophys Res 112:B08303. doi:10.1029/2006JB004513

McFadden P, Drummond B, Kravis S (1986) The Nth-root stack—theory, applications, and examples. Geophysics 51:1879–1892. doi:10.1190/1.1442045

McMechan G (1983) Migration by extrapolation of time-dependent boundary values. Geophys Prospect 31:413–420. doi:10.1111/j.1365-2478.1983.tb01060.x

Mercier J, Bostock M, Audet P, Gaherty J, Garnero E, Revenaugh J (2008) The teleseismic signature of fossil subduction: northwestern Canada. J Geophys Res 113:B04308. doi:10.1029/2007JB005127

Mohan G, Rai S (1992) Imaging of seismic scatterers beneath the Gauribidanur (GBA) array. Phys Earth Planet Inter 71:36–45. doi:10.1016/0031-9201(92)90026-R

Muirhead K, Datt R (1976) N-th root process applied to seismic array data. Geophys J R Astron Soc 47: 197–210

Müller G (1985) The reflectivity method—a tutorial. Geophysics—Z Geophysik 58:53–174

Mykkeltveit S, Astebol K, Doornbos D, Husebye E (1983) Seismic array configuration optimization. Bull Seismol Soc Am 73:173–186

Neele F, deRegt H, VanDecar J (1997) Gross errors in upper-mantle discontinuity topography from underside reflection data. Geophys J Int 129:194–204. doi:10.1111/j.1365-246X.1997.tb00949.x

Neidell N, Taner M (1971) Semblance and other coherency measures for multichannel data. Geophysics 36:482–497. doi:10.1190/1.1440186

Niazi M (1969) Use of source arrays in studies of regional structure. Bull Seismol Soc Am 59:1631–1643

Reasoner C, Revenaugh J (1999) Short-period *P* wave constraints on D″ reflectivity. J Geophys Res 104:955–961. doi:10.1029/1998JB900053

Revenaugh J (1995a) A scattered-wave image of subduction beneath the transverse ranges. Science 268:1888–1892. doi:10.1126/science.268.5219.1888

Revenaugh J (1995b) Relation of the 1992 Landers, California, earthquake sequence to seismic scattering. Science 270:1344–1347. doi:10.1126/science.270.5240.1344

Revenaugh J, Mendoza H (1996) Mapping shallow heterogeneity with teleseismic P to Rg scattered waves. Bull Seismol Soc Am 86:1194–1199

Roecker S (2001) Constraints on the crust and upper mantle of the Kyrgyz Tien Shan from the preliminary analysis of GHENGIS broad-band seismic data. Geologiya I Geofizika 42:1554–1565

Rost S, Garnero E (2004) Array seismology advances research into earth's interior. EOS 85(301):305–306

Rost S, Thomas C (2002) Array seismology: methods and applications. Rev Geophys 40:1008. doi:10.1029/2000RG000100

Rost S, Thorne MS, Garnero EJ (2006) Imaging global seismic phase arrivals by stacking array processed short-period data. Seismol Res Lett 77:697–707. doi:10.1785/gssrl.77.6.697

Rost S, Garnero E, Williams Q (2008) Seismic array detection of subducted oceanic crust in the lower mantle. J Geophys Res 113:B06303. doi:10.1029/2007JB005263

Scherbaum F, Gillard D, Deichmann N (1991) Slowness power spectrum analysis of the coda composition of 2 microearthquake clusters in northern Switzerland. Phys Earth Planet Inter 67:137–161. doi:10.1016/0031-9201(91)90067-R

Scherbaum F, Krüger F, Weber M (1997) Double beam imaging: mapping lower mantle heterogeneities using combinations of source and receiver arrays. J Geophys Res 102:507–522. doi:10.1029/96JB03115

Schimmel M, Paulssen H (1997) Noise reduction and detection of weak, coherent signals through phase-weighted stacks. Geophys J Int 130:497–505. doi:10.1111/j.1365-246X.1997.tb05664.x

Schmerr N, Garnero E (2006) Investigation of upper mantle discontinuity structure beneath the central Pacific using SS precursors. J Geophys Res 111:B08305. doi:10.1029/2005JB004197

Schneider W (1978) Integral formulation for migration in 2 and 3 dimensions. Geophysics 43:49–76. doi:10.1190/1.1440828

Schweitzer J, Fyen J, Mykkeltveit S, Kvaerna T (2002) Seismic arrays: in new manual of seismological observatory practice—NMSOP. IASPEI, pp 481–532

Sheriff R (1980) Nomogram for fresnel-zone calculation. Geophysics 45:968–972. doi:10.1190/1.1441101

Sheriff RE, Geldart LP (1995) Exploration seismology, 2nd edn. Cambridge University Press, Cambridge

Spudich P, Bostwick T (1987) Studies of the seismic coda using an earthquake cluster as a deeply buried seismograph array. J Geophys Res 92:10526–10546. doi:10.1029/JB092iB10p10526

Stammler K (1993) Seismichandler—programmable multichannel data handler for interactive and automatic processing of seismological analysis. Comput Geosci 19:135–140. doi:10.1016/0098-3004(93)90110-Q

Takahashi T (1995) Prestack migration using arrival angle information. Geophysics 60:154–163. doi:10.1190/1.1443742

Tarenghi M (2008) The Atacama large millimeter/submillimeter array: overview and status. Astrophys Space Sci 313:1–7. doi:10.1007/s10509-007-9602-9

Thomas C, Billen M (2009) Upper mantle structure along a profile in the southwest Pacific. Geophys J Int 176(1):13–125

Thomas C, Weber M, Wicks C, Scherbaum F (1999) Small scatterers in the lower mantle observed at German broadband arrays. J Geophys Res 104:15073–15088. doi:10.1029/1999JB900128

Thomas C, Garnero E, Lay T (2004) High-resolution imaging of lowermost mantle structure under the Cocos plate. J Geophys Res 109:B08307. doi:10.1029/2004JB003013

Tkalčić H, Flanagan M, Cormier V (2006) Observation of near-podal P′P′ precursors: Evidence for back scattering from the 150–220 km zone in the earth's upper mantle. Geophys Res Lett 33:L03305. doi:10.1029/2005GL024626

Vernon F (1994) The Kyrgyz seismic network. IRIS Newsl XIII:7–8

Vidale J, Earle P (2000) Fine-scale heterogeneity in the earth's inner core. Nature 404:273–275. doi:10.1038/35005059

Wang P, de Hoop M, van der Hilst R, Ma P, Tenorio L (2006) Imaging of structure at and near the core mantle boundary using a generalized radon transform: 1. Construction of image gathers. J Geophys Res 111:B12304. doi:10.1029/2005JB004241

Weber M, Davis J (1990) Evidence of a laterally variable lower mantle structure from *P*-waves and *S*-waves. Geophys J Int 102:231–255. doi:10.1111/j.1365-246X.1990.tb00544.x

Weber M, Wicks C (1996) Reflections from a distant subduction zone. Geophys Res Lett 23:1453–1456. doi:10.1029/96GL01322

Wessel P, Smith W (1998) New, improved version of the generic mapping tools. EOS 79:579. doi:10.1029/98EO00426

Williams E, Maynard J, Skudrzyk E (1980) Sound source reconstructions using a microphone array. J Acoust Soc Am 68:340–344. doi:10.1121/1.384602

Zhao L, Chevrot S (2003) SS-wave sensitivity to upper mantle structure: Implications for the mapping of transition zone discontinuity topographies. Geophys Res Lett 30:1590. doi:10.1029/2003GL017223